Mathematical Modelling for Sustainable Engineering
https://www.acadlore.com/journals/MMSE

Computational Assessment of Vascular Heat-Sink Effects in Radiofrequency and Microwave Ablation of Liver Tumors

Muhammet Kaan Yeşilyurt[1,2], Mansur Mustafaoğlu[2,3*]

[1] Department of Mechanical Engineering, Faculty of Engineering, Atatürk University, 25040 Erzurum, Turkey
[2] Department of Nano-Science and Nano-Engineering, Institute of Science, Atatürk University, 25040 Erzurum, Turkey
[3] Department of Emergency Aid and Disaster Management, Faculty of Health Sciences, Erzurum Technical University, 25100 Erzurum, Turkey

[*] Correspondence: Mansur Mustafaoğlu (mansour@atauni.edu.tr)

Received: 11-09-2025 **Revised:** 12-18-2025 **Accepted:** 12-27-2025

Citation: M. K. Yeşilyurt and M. Mustafaoğlu, "Computational assessment of vascular heat-sink effects in radiofrequency and microwave ablation of liver tumors," *Math. Model. Sustain. Eng.*, vol. 1, no. 2, pp. 102–114, 2025. https://doi.org/10.56578/mmse010204.

Abstract: Thermal ablation has been widely adopted for the treatment of liver tumors; however, treatment efficacy can be substantially compromised by vascular heat-sink effects arising from adjacent blood vessels. In this study, a comprehensive investigation was conducted to quantitatively compare radiofrequency ablation and microwave ablation with specific emphasis on vessel-induced thermal dissipation. A coupled multiphysics finite element framework was developed in COMSOL Multiphysics. For radiofrequency ablation, quasi-static electric currents were coupled with the bioheat transfer equation to model Joule heating, whereas for microwave ablation, electromagnetic wave propagation was coupled with bioheat transfer to represent dielectric heating. Thermal tissue injury was evaluated using an Arrhenius damage formulation, and treatment outcome was quantified in terms of necrotic volume fraction after a simulated ablation duration of 600 s. Two configurations were examined: a baseline liver tissue domain without vascular structures and a vascularized domain incorporating a representative 5 mm-diameter blood vessel positioned in proximity to the ablation applicator. In addition, a verification scenario was implemented by reproducing reported operating conditions from the literature to confirm the predicted magnitude of vessel-related lesion attenuation under a consistent necrosis definition. The results demonstrate that the presence of a blood vessel leads to a markedly greater reduction in predicted necrotic volume for radiofrequency ablation (34.08%) than for microwave ablation (18.96%). Furthermore, the simulated ablation morphology was found to be more spherical in radiofrequency ablation and more axially elongated in microwave ablation. These findings indicate that vascular heat-sink effects differentially influence ablation modalities and should be explicitly considered during modality selection and parameter optimization, particularly for tumors located adjacent to major hepatic vessels. The proposed computational framework provides a robust and extensible platform for pre-procedural planning and comparative evaluation of thermal ablation strategies in vascularized hepatic tissue.

Keywords: Liver tumor; Thermal ablation; Radiofrequency ablation; Microwave ablation; Vascular heat-sink effect

1 Introduction

Liver cancer is a significant disease group associated with high morbidity and mortality. Radiofrequency ablation and microwave ablation are widely used minimally invasive thermal methods, aiming to raise the tumor tissue to cytotoxic temperatures (typically $\geq$50 °C) and cause coagulation necrosis without damaging the adjacent healthy parenchyma [1]. However, the liver has significant vascularity which can alter heat transfer and limit ablation effectiveness particularly in the vicinity of large vessels. Intravascular blood flow constitutes a convective heat transport that disrupts the temperature field through local heat-sink effects [2], which can result in inadequate ablation and an increased risk of local recurrence. Therefore, quantitative modeling of the vascular effect is a crucial requirement for method selection and determination of application parameters. Microwave ablation and radiofrequency ablation differ from one another in terms of the frequency of electromagnetic waves used, and consequently, tissue penetration, the heat generation mechanism, and clinical application areas. Microwave ablation uses microwave energy in the 915

MHz–2.45 GHz range and can provide a deeper and faster increase in heat within the tissue by directly vibrating water molecules. Furthermore, microwave ablation is less affected by the electrical conductivity of surrounding tissues and offers a homogeneous thermal distribution. This allows for effective ablation of large and heterogeneous tumors but also brings on a higher risk of damaging surrounding healthy tissues.

Radiofrequency ablation, on the other hand, typically uses radiofrequency energy in the 300 kHz–1 MHz range and creates a more localized heating effect. It is sensitive to the electrical conductivity of surrounding tissues, which provides more controlled and targeted heat generation in specific areas. This can be considered a significant advantage, especially in the treatment of small and well-defined lesions but it has lower effectiveness in areas with high fat content or tissues with low conductivity. Additionally, because the thermal effect obtained with radiofrequency ablation is usually concentrated in a more limited area, treatment time may be longer for large tumors. The choice of application should be determined according to the patient's condition, the characteristics of the target tissue, and the treatment requirements. Hybrid approaches combining the advantages of both methods are also being investigated for optimal results. Several studies have shown the potential of numerical modeling to contribute to clinical parameter selection.

Tungjitkusolmun et al. [3] investigated one of the early and referenced contributions to the three-dimensional finite element method modeling of radiofrequency ablation in liver tumors. The intratissue heat distribution and lesion geometry were predicted through the coupling of electrical and thermal fields around the electrode and the role of electrode placement and energy parameters on lesion formation was addressed. Vaidya et al. [4] computationally investigated the cooling effect of vessels during liver radiofrequency ablation and the coagulation processes that may accompany it. The study reveals that vessel-derived cooling can limit lesion development by reducing the temperature field; changes in flow conditions with coagulation can modify this effect. This approach supports the need to consider more realistic boundary conditions and time-dependent biophysical processes for radiofrequency ablation in the vicinity of vessels. Consequently, approximating model inputs to clinical physiology can directly affect lesion prediction.

Van Erp et al. [5] conducted a systematic review of computational modeling of liver thermal ablation sites on the axes of accuracy, predictability, and clinical usability. In addition, the impact of material properties, perfusion, boundary conditions, and validation strategies on the results was discussed. By assessing the assumptions the models used for patient-based planning and procedure optimization, a direct reference for reporting the assumptions used in the present study and justifying the validation steps was drawn. Alemaryeen and Noghanian [6] addressed the relationship between electromagnetic energy absorption and heat generation and discussed thermal analysis methods across a wide range of applications. Although it does not directly focus on liver ablation, the methods and criteria used in the computational analysis of electromagnetically induced heating provide a conceptual background for microwave ablation modeling. Bendahmane et al. [7] presented the mathematical analysis and numerical solution of a coupled electro-thermal radiofrequency ablation model for cardiac tissue. The model aims to represent the biophysical processes of radiofrequency ablation more consistently by considering the time-dependent interaction of the electrical field, tissue heating, and conductivity change together. The results suggest that the effect of the electrical field on the tissue properties should also be considered along with the heat conduction.

Fang et al. [8] addressed the optimization of the radiofrequency ablation protocol in liver tumors surrounded by complex vascular geometries by using response surface methodology and computational modeling together. Parameter sets were determined to reduce the negative impact of vascular cooling and increase ablation efficacy. The study showed that geometric and hemodynamic uncertainties should be considered as a separate sensitivity heading in optimization since neglecting the vascular effect can mislead optimal parameter selections, which suggests that patient-based planning is necessary. Lim et al. [9] investigated the effect of input waveform pattern and the presence of large vessels on lesion formation in radiofrequency ablation using finite element analysis. The study showed that source definition (excitation mode) can alter the temperature field and, therefore, the temporal character of the energy input is not a secondary detail in terms of model accuracy. It was also reported that the vessel proximity can significantly affect the results since the lesion boundaries can be irregular due to the cooling effect of large vessels. De Vita et al. [10] evaluated the heat-sink effects occurring during microwave ablation in hepatic tissue using experimental and computational methods. The presence of large vessels was confirmed to have altered heat distribution and that it can have a limiting effect on ablation volume and homogeneity despite the higher power density and different energy transfer mechanism. The results are indicative of the need to report and analyze vascular conditions.

Zhang et al. [11] numerically investigated the effect of target geometry on heat accumulation and necrosis development in pulsed radiofrequency ablation and reported that thermal damage is controlled not only by power and duration but also by the characteristic length scales of the target, which highlights the necessity of selecting energy settings according to tumor size. Mohammadpour and Firoozabadi [12] numerically modeled ablation in porous liver tissue with high-intensity focused ultrasound and investigated the heat transfer and hemodynamic effects together in relation to blood flow and tissue structure. The findings supported the idea that the size and shape of the ablation site, which is a common determinant in different thermal modalities, is dependent on the redistribution

of heat transfer by tissue-flow interaction. As a matter of fact, the inclusion of hemodynamic conditions in the numerical model emerges as a common accuracy requirement for different energy sources. Literature studies clearly show that thermal interactions around vessels are not limited to the liver and that intravascular heating dynamics are determined by similar physical mechanisms in different clinical applications. Choi et al. [13] mathematically modeled radiofrequency ablation used in varicose vein treatment and investigated the thermal interactions between tissue heating and vascular structure in detail. This study reveals that the heat distribution generated by radiofrequency energy in vessels can be decisive in terms of efficacy and risk of complications, and provides a methodological basis for a model-based protocol development approach.

Computational studies for microwave ablation also highlight the need to consider electromagnetic heat generation and blood flow-dependent transport together. Rattanadecho and Keangin [14] numerically investigated the microwave ablation process in liver tissue, comparing single- and double-slot antenna configurations and demonstrating that blood flow can significantly alter tissue damage through thermal distribution. These findings show that considering antenna geometry and application parameters together with vascular effects in microwave ablation is critical in terms of lesion volume and homogeneity. Therefore, evaluating the modality-specific source definition and hemodynamic conditions within a common framework becomes a fundamental component of optimization studies. The topological properties of the vessel networks reveal that the heat-sink effects have a more complex structure than a single vessel proximity problem. Shao et al. [15] reported that the number of vessel branches, total vessel volume, and needle-vessel mean distance amplify this effect. However, in multi-scale modeling studies, the issue of how the cooling effect changes depending on the orientation of isolated vessels has been addressed to a limited extent [16–18]. While current studies cumulatively highlight the importance of vascular cooling, research that examines the susceptibility of radiofrequency ablation and microwave ablation to vascular cooling under common damage measures and in comparable scenarios remains limited.

This study investigates the vascular heat-sink effects in radiofrequency ablation and microwave ablation through numerical analysis of how the presence of a representative vessel adjacent to the applicator modifies the temperature field and the predicted thermal damage under comparable treatment times. By evaluating both modalities using the same Arrhenius-based damage metric, the analysis clarifies modality-dependent susceptibility to vascular cooling and provides quantitative inputs for treatment planning in lesions near large vessels.

2 Materials and Methods

2.1 Numerical Modeling Approach

Simulation of thermal treatment methods such as radiofrequency ablation and microwave ablation requires the simultaneous solution of bioheat transfer equations with electric current and electromagnetic wave equations. In this study, radiofrequency ablation and microwave ablation used in the thermal treatment of liver tumors were computationally modeled to quantitatively investigate the vascular heat-sink effects. In radiofrequency, energy is transferred to the tissue via an electric current transmitted through an electrode, and a temperature increase occurs through Joule heating (loss of resistance) in the tissue. In microwave ablation, the electromagnetic field generates volumetric heat in the tissue through dielectric losses. Since these two mechanisms can produce different temperature gradients and necrosis geometries in the same biophysical environment, the models were established within a comparative framework.

2.2 Geometry and Network Structure

The liver is idealized as a rectangular prism volume (Figure 1). Due to the applicator physics, the radiofrequency problem is solved in three dimensions because the electric potential and current distribution around the electrode are fully three-dimensional. The microwave ablation problem is solved in a two-dimensional axially symmetric plane based on the axial symmetry of the coaxial antenna [19]. The vessel diameter is taken as 5 mm. For the main radiofrequency–microwave ablation comparison, the application time is 600 s; the radiofrequency electrode potential is set to 25 V, and the microwave ablation operating frequency and supplied power are set to 2.45 GHz and 10 W, respectively. In addition, a separate verification case reproduces the operating conditions used by Pillai et al. [20] by applying 33 V for radiofrequency and 25 W for microwave ablation for the same duration. The finite element mesh is constructed to include local refinement around the applicator and vessel (Figure 2) to capture steep field and temperature gradients.

The numerical setup was informed by the COMSOL Hepatic Tumor Ablation tutorial, which represents tissue as a large cylinder with boundary temperature fixed at 37 °C and applies a prescribed electrode potential of 22 V for the radiofrequency case [21]. In the present study, the liver is represented as a rectangular prism to enable direct comparison with a two-dimensional axisymmetric microwave domain; the initial temperature is set to 37 °C, and the outer boundaries are treated with temperature, symmetry, and insulation conditions consistent with Figure 1 rather than a uniform fixed-temperature boundary. The baseline radiofrequency potential is set to 25 V for the main comparison, while a separate verification case uses 33 V and 25 W to match the literature conditions used for model

checking. This description distinguishes geometry- and boundary-driven differences from modality-driven differences in the results.

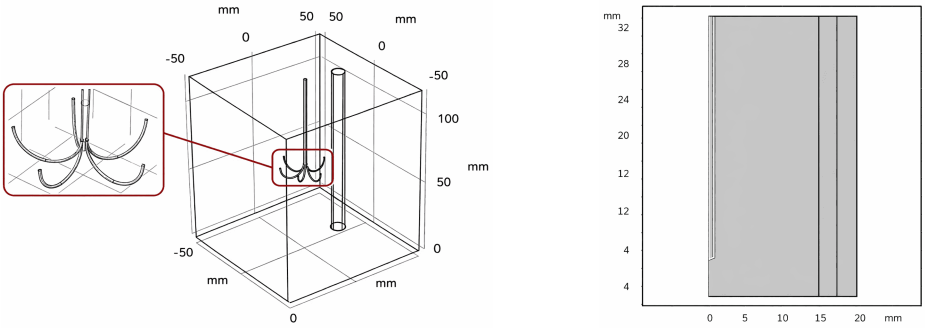

(a) (b)

Figure 1. Physical model: (a) radiofrequency modeling; (b) microwave modeling

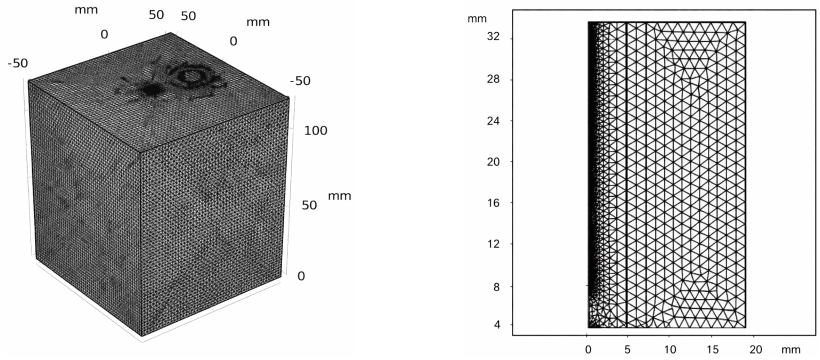

(a) (b)

Figure 2. Mesh structure: (a) microwave modeling; (b) radiofrequency modeling

2.3 Heat Transfer Model

Accurate modeling of heat transfer and analysis of temperature changes in the target tissue are critical for determining the effectiveness of heat therapy. To address heat transfer mechanisms more realistically, the tissue is considered as a porous medium. Heat transfer in tissues has four basic components: conduction, convective heat transfer via blood flow, metabolic heat production, and external heat flux.

• Conduction is the most fundamental mechanism determining temperature distribution within the tissue and is typically modeled by Fourier's equation for heat conduction.

• Blood circulation is a means of convective heat transfer, which alters the temperature distribution within the tissue. As a result, highly vascularized tissues may tend to stay cool whereas tissues with low blood flow may heat up more.

• Metabolic heat production, a consequence of the normal physiological activities of cells, can be greater at certain abnormal cellular structures, particularly tumor tissues.

• The externally applied heat flux (such as microwave or radiofrequency energy) directly determines the effectiveness of the treatment and must be carefully controlled to create sufficient thermal damage in the target tissue.

Consequently, accurate modeling of heat transfer processes in biological tissues is crucial for the effectiveness of heat therapy methods. Incorrect modeling can lead to damage to surrounding healthy tissues due to insufficient or excessive heating. Various approaches have been developed to model heat transfer in body tissues, the most common and widely accepted of which is the Pennes bioheat transfer model [22]. The Pennes model is a fundamental reference model in the field of biomedicine for thermal treatments (radiofrequency ablation, microwave ablation, laser therapy, etc.) and provides an important basis for explaining tissue temperature changes.

The tissue temperature field is defined by the Pennes bioheat transfer equation given in Eq. (1) [22]. This equation combines heat transfer by conduction, heat transfer by perfusion, metabolic heat production, and volumetric heat

source due to externally applied energy. The basic equation of the model is as follows [23, 24]:

$$\rho c \frac{\partial T}{\partial t} = k\nabla^2 T + \rho_b c_b w\,(T_b - T) + q_m + q_a \tag{1}$$

where, ρ_b represents the density of the blood, c_b represents the specific heat of the blood, k represents the heat conduction coefficient, w represents the blood perfusion rate, T represents the tissue temperature, T_b represents blood temperature, q_m denotes the metabolic heat production, and q_a denotes the external heat flux due to radio or microwaves. However, the model also has some limitations. For example, it does not fully account for the orientations of vascular structures and the cooling effect of individual vessels. Furthermore, while it considers the macroscopic effect of blood flow, it neglects details at the microscopic level.

2.4 Thermal Damage and Necrosis Criteria

Thermal damage to tissue and blood was assessed using the Arrhenius model, a commonly used kinetic model, as shown in Eq. (2). Initially, undamaged tissue was assumed by taking the initial condition $\omega(x, 0) = 1, (\Omega = 0)$. The Arrhenius parameters, frequency factor (A), activation energy (ΔEa), and ideal gas constant (R) are given in Table 1. The necrosis threshold was defined by the survival rate satisfying $\omega(x, t) < e - 1$ (0.37 or 37% survival rate); this threshold is commonly used to denote irreversible damage and to delineate the thermal coagulation zone [25]. For the current study, the lethal temperature threshold for necrosis was assumed to be 50 °C, consistent with conventional indicators [21]. For reporting and comparison, "tissue necrosis" in Table 2 and subsequent figures denotes the volume fraction of the modeled tissue domain that satisfies $\omega < e - 1$ at t = 600 s. This model plays a critical role in calculating treatment efficacy and protecting healthy tissues [25].

$$\frac{\partial \omega(\vec{x}, t)}{\partial t} = -A \exp\left(\frac{-\Delta E_a}{RT(\vec{x}, t)}\right) \omega(\vec{x}, t) \tag{2}$$

In coaxial antennas, the propagation of electromagnetic waves is characterized by transverse electromagnetic fields:

$$E = e_r \frac{C}{r} \mathrm{e}^{j(\omega t - kz)} \tag{3}$$

$$H = e_\varphi \frac{c}{rZ} \mathrm{e}^{j(\omega t - kz)}) \tag{4}$$

$$P_{av} = \int_{r_{\text{inner}}}^{r_{\text{outer}}} \mathrm{Re}\left(\frac{1}{2} E \times H^*\right) 2\pi r dr = \mathrm{e}_z \pi \frac{C^2}{Z} \ln\left(\frac{r_{\text{outer}}}{r_{\text{inner}}}\right) \tag{5}$$

In Eqs. (3)–(5), wave propagation is taken along the antenna axis (z-direction). For a transverse electromagnetic mode in a coaxial structure, the electric field is predominantly radial and the magnetic field is predominantly azimuthal, with magnitudes that vary with radius. The propagation constant and characteristic impedance depend on the dielectric properties and the inner/outer conductor radii [19].

$$k_0 = \frac{w}{c_0} \tag{6}$$

Eq. (8) was used to model the microwave antenna [24, 26, 27].

$$\nabla^2 \boldsymbol{E} - \mu_r \mathrm{k}_0^2 \left(\varepsilon_r - \frac{\mathrm{j}\sigma}{\omega \varepsilon_0}\right) \boldsymbol{E} = 0 \tag{7}$$

where, E denotes the electric field vector, k_0 denotes the vacuum propagation constant which is given in Eq. (7), ε_0 is the vacuum dielectric constant (8.854×10^{-12} F/m), ε_r is the relative permittivity, μ_r is the tissue permeability, σ is the electrical conductivity, and ω is the angular frequency. The electromagnetic boundary condition for metallic surfaces is defined in Eq. (8).

$$n \times E = 0 \tag{8}$$

The antenna feed is implemented as a port boundary condition that imposes the specified operating frequency and input power. The electromagnetic field solution yields a local loss density in tissue, which is transferred to the thermal model as a volumetric heat source term, as shown in Eq. (9) [19].

$$n \times \sqrt{\varepsilon} E - \sqrt{\mu} H_\varphi = -2\sqrt{\mu} H_{\varphi 0} \tag{9}$$

$$H_{\varphi 0} = \frac{\sqrt{\frac{P_{\text{av}} Z}{\pi r \ln\left(\frac{r_{\text{outer}}}{r_{\text{inner}}}\right)}}}{r} \tag{10}$$

Table 1. Material properties [4]

Region	Material Property	Value
Tissue	ρ (kg·m^{-3})	1079 [28]
	C (J·kg^{-1}·K^{-1})	3540 [28]
	$k(T(^\circ\mathrm{C}))$ (W·m^{-1}·K^{-1})	$4.69 \times 10^{-1} + 1.16 \times 10^{-3} \times T$ [29]
		Healthy tissue
	$\sigma(T(^\circ\mathrm{C}))$ (S·m^{-1})	$-1.26 \times 10^{-7} \times T^4 + 2.57 \times 10^{-5} \times T^3$
	Healthy tissue	$-1.84 \times 10^{-3} \times T^2 + 6.35 \times 10^{-2} \times T - 4.79 \times 10^{-1}$ [30]
	$k(T(^\circ\mathrm{C}), r_{\mathrm{tum}})$	0.561: $r_{\mathrm{tum}} < 3$
	W(m^{-1}·K^{-1})	$0.419 + 3.91 \times 10^{-3} \times T$: $r_{\mathrm{tum}} \geq 3$ [29]
		Tumor tissue
	$\sigma(T(^\circ\mathrm{C}))$ (S·m^{-1})	$-1.26 \times 10^{-7} \times T^4 + 2.57 \times 10^{-5} \times T^3$
	Tumor tissue	$-1.84 \times 10^{-3} \times T^2 + 6.35 \times 10^{-2} \times T - 0.378$ [31]
	A (s^{-1})	3.1×10^{98}
	ΔE_a (J)	6.285×10^5
	R (J·mol^{-1}·K^{-1})	8.314
Blood	ρ (kg·m^{-3})	1050 [28]
	C (J·kg^{-1}·K^{-1})	3617 [28]
	k(T($^\circ$C)) (W·m^{-1}·K^{-1})	$0.552 - 2.26 \times 10^{-3} \times (37 - T)$ [32]
	$\sigma(T(^\circ\mathrm{C}))$ (S·m^{-1})	$100 \times (326.0 - 5.63 \times T)^{-1}$ [33]
		Healthy blood
	σ (S·m^{-1}) coagulated blood	0.3114 [34]
	A (s^{-1})	7.66×10^{98}
	ΔE_a (J)	4.225×10^5
	R (J·mol^{-1}·K^{-1})	8.314
RF	ρ (kg·m^{-3})	1
	C (J·kg^{-1}·K^{-1})	1000
Needle	k (W·m^{-1}·K^{-1})	0.02
	σ (S·m^{-1})	1×10^7
Phantom	ρ (kg·m^{-3})	1033 [35]
	C (J·kg^{-1}·K^{-1})	3939 [35]
	k (W·m^{-1}·K^{-1})	0.59 [35]
	σ (S·m^{-1})	1

Table 2. Confirmation of the results of the current study and the study by Pillai et al. [20]

Method	Tissue Necrosis (With Vessel)	Tissue Necrosis (Without Vessel)	Heat-Sink Effects of This Study (%)	Heat-Sink Effects(%) [20]
Radiofrequency	0.386	0.585	34.08	39
Microwave	0.391	0.483	18.96	23

2.5 Electromagnetic and Electric Field Models

Electromagnetic waves, particularly high-frequency microwaves, move free charge carriers (such as electrons) in tissue, and this movement generates heat. This process is known as dielectric loss, and the energy resulting from this loss is converted into heat in the tissue. Resistive heat arises from the interaction between the electromagnetic field of microwave energy and the electrical properties of the tissue. Microwaves generate heat according to the electrical conductivity of tissues; this conductivity depends on the water content and ionized properties of the tissue. The microwave ablation antenna is modeled as a dielectric-filled coaxial structure operating in the transverse electromagnetic mode, and the feed is defined using a port boundary condition, as shown in Eqs. (3)–(11). Metallic surfaces are treated using the electromagnetic boundary condition in Eq. (9). The volumetric heat generation term used in the bioheat equation is obtained from the electromagnetic loss density computed in tissue, as shown in Eq. (11) [19].

$$Q_{\text{ext}} = \frac{1}{2} \operatorname{Re}\left[(\sigma - j\omega\varepsilon)E \cdot E^*\right] \tag{11}$$

Radiofrequency current is generally more easily transmitted by conductive structures such as blood vessels and tissues with high water content, which increases heat generation during the treatment process. Therefore, the effect of radiofrequency energy is of great importance, especially in applications such as cancer treatment and tumor ablation,

in terms of the energy applied to the tissue and the resulting temperature increase. In the radiofrequency model, the electric potential field and the associated current density are solved with the electric current equation, as shown in Eq. (12), and Joule heating is connected to the bioheat equation as a volumetric heat source.

$$Q_j = -\nabla \cdot (\sigma \nabla V - J^e) \tag{12}$$

where, V is the electric potential (V), σ is the electrical conductivity (S/m), and J^e is an externally prescribed current density $\left(\mathrm{A/m^2}\right)$ when applicable. The radiofrequency model is solved in the quasi-static regime using the electric currents formulation, in which displacement currents are neglected relative to conduction currents over the domain size of interest. The resulting Joule heating term is coupled to the bioheat equation to compute the transient temperature field, which is then used to evaluate Arrhenius damage. This sequential coupling can be summarized as "electric field → volumetric heat generation → temperature field → Arrhenius damage" [21].

2.6 Material Properties and Temperature Dependence

To more accurately represent the behavior of real biological tissues, the thermal conductivity $k(T)$ and electrical conductivity $\sigma(T)$ of tissue and blood are defined as temperature-dependent functions. This choice is particularly important because the change in electrical conductivity in the ablation temperature range creates feedback via Joule heating.

In contrast, density and specific heat were assumed to be constant. While this simplification facilitates solution stability and parameter management, the assumption that these parameters are constant in certain temperature ranges may limit the accuracy of the model because it does not represent additional changes in tissue properties (e.g., tissue vaporization or structural transformations) at high temperature levels; this assumption should be taken into account in the interpretations. The material values used for the needle/antenna and phantom are also summarized in Table 1.

In the thermal solution, the initial temperature was taken as 37 °C. In contrast to the reference COMSOL hepatic model, which assumes a large cylindrical domain with an external boundary held at 37 °C throughout the procedure [21], the present study applies temperature, symmetry, and insulation boundary conditions on the outer surfaces to represent the simplified geometry and to focus the analysis on local heating near the applicator and vessel. For radiofrequency, the outer tissue boundaries were connected to a ground reference and the electrode surface was driven by a prescribed potential. For microwave ablation. the antenna feed was defined at 2.45 GHz using a port boundary condition with a prescribed input power; the resulting electromagnetic loss density was converted to a thermal source term. Unless otherwise stated, the main comparison uses $V_{RF} = 25\mathrm{V}$ and P_{MW} = 10 W for 600 s ; the verification case uses $V_{RF} = 33$ V and P_{MN} = 25 W in line with Pillai et al. [20]. These boundary condition definitions establish a consistent framework for comparing modality-dependent heating while preserving the physical character of energy delivery in radiofrequency and microwave ablation.

2.7 Numerical Solution and Verification

All multi-physics problems were solved using the finite element method in the COMSOL Multiphysics environment. In the solution flow, the electric current or electromagnetic wave equations were solved first, and the resulting power/heat generation terms were related to the bioheat equation to calculate the time-dependent temperature field. A time step of 0.1 s was used in the thermal solution; a tolerance of 10^{-6} was taken for electromagnetic solutions, and convergence was limited to 5000 iteration steps. The reliability of the model was evaluated by comparison with the ex vivo setup reported by Pillai et al. [20]; in the validation, the heat-sink effects were defined through the difference between the calculated necrosis magnitudes in the presence and absence of vessels, and consistency was checked with the ratios given in Table 2. This validation provides the necessary level of confidence to proceed to the numerical basis of subsequent comparative radiofrequency–microwave ablation analyses.

3 Results and Discussion

The heat-sink effects occur when heat is removed by convection within the vessel lumen and by enhanced heat transfer around the vessel wall, which locally suppresses the temperature field. This mechanism increases the volume below threshold temperatures in the target region and reduces Arrhenius-based damage accumulation; therefore, the necrosis volume can be significantly reduced in the vicinity of the vessel. The magnitude of this reduction depends on the modality and the applied heating rate; for microwave systems, rapid volumetric heating can partially overcome vessel-driven heat-sink effects under certain operating conditions [19]. In this context, defining the heat-sink effects through necrosis provides a validation metric directly related to clinical outcome.

Table 2 summarizes the calculated necrosis values for the presence and absence of a vessel and the derived heat-sink effects. In radiofrequency treatment, the necrosis volume fraction changes from 0.386 (with vessel to 0.585 (without vessel); in microwave ablation, it changes from 0.391 to 0.483. Using the definition $\eta = (\mathrm{N_{no\text{-}vessel}} - \mathrm{N_{vesel}}) / \mathrm{N_{no\text{-}vesel}} \times 100\%$, the heat-sink effects are 34.08% for radiofrequency ablation and 18.96% for

microwave ablation in the present model. Pillai et al. [20] reported corresponding values of 39% and 23%, respectively, under comparable operating conditions.

3.1 Temperature and Necrosis Distributions in the Absence of Blood Vessels

In the reference case where no blood vessels are present, the temperature and necrosis areas for radiofrequency are given in Figure 3 and Figure 4 and for microwave in Figure 5 and Figure 6. In both methods, the temperature gradient weakens as the distance from the heat source increases, and consequently, the necrosis area narrows. This trend is a natural consequence of the geometric damping of heat conduction and diffusion into the surrounding tissue. The fact that the necrosis geometry shows a more spherical character for radiofrequency and a more elliptical character for microwave under the same conditions can be explained by the difference in energy accumulation and field distribution depending on the application physics.

Figure 3 shows the spatial boundaries of the necrotic region formed under radiofrequency application. The contour reveals that the damage is concentrated around the heat source and rapidly weakens with increasing distance. This distribution points to a more symmetrical necrotic volume, expected under conditions where isotropic heat diffusion is dominant.

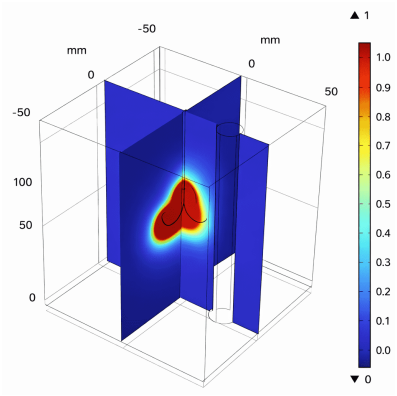

Figure 3. Contour of tissue necrosis in radiofrequency thermotherapy

Figure 4 shows the temperature field corresponding to radiofrequency application via cross-sections. The temperature is observed to reach a maximum around the electrode and decrease steadily in the surrounding tissue; this pattern is the key input determining the location of the necrosis contour. This localization of the temperature field indicates that the boundaries of the ablation area are controlled by energy input and tissue properties.

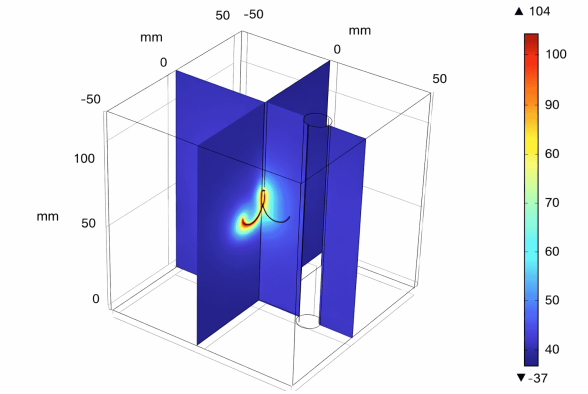

Figure 4. Temperature contour in radiofrequency thermotherapy

Figure 5 shows that necrosis exhibits a more directional distribution in microwave treatment. Damage is observed to be concentrated around the antenna, and the geometry tends towards a more elliptical volume compared to radiofrequency. This result is consistent with the way energy is stored in tissue using a microwave field.

Figure 6 shows that in microwave therapy, the temperature gradient is sharper around the antenna and the temperature gradually decreases in the surrounding tissue. Since the shape of the temperature field directly determines the extent of necrosis volume, such distributions are critical for treatment adequacy, especially in borderline regions.

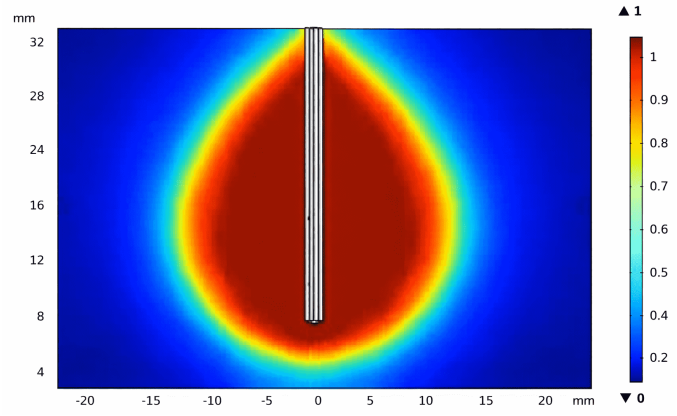

Figure 5. Contour of tissue necrosis in microwave heat therapy

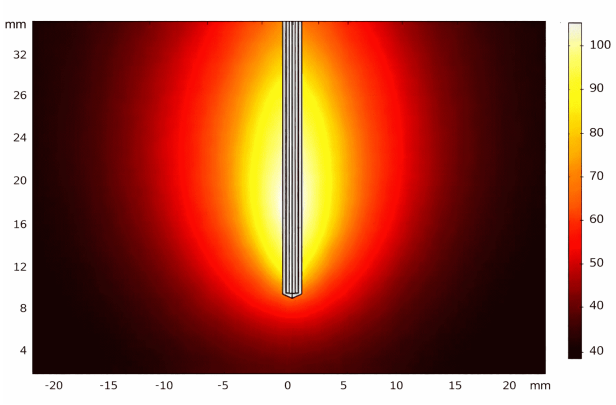

Figure 6. Temperature distribution in microwave heat therapy

3.2 Threshold Temperature Volume and Damage Development Over Time

Figure 7 shows the region reaching 50 °C at 10 minutes in microwave application. This representation reveals that the volume remaining above a certain threshold temperature is locally limited and that heating is concentrated around the antenna; thus, it provides a direct measure for evaluating the relationship between clinical target volume and application time/power.

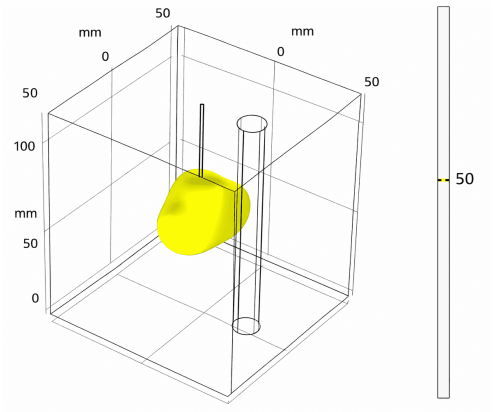

Figure 7. Region reaching 50 °C at 10 minutes

Figure 8 shows the change in damage fraction over time at different distances in microwave application in the absence of vessels. The faster rise of the curves near the source indicates that damage accumulation is sensitive to both temperature level and exposure time, and the thermal effect decreases rapidly as the distance increases. This finding suggests that errors in target placement or positional uncertainties may affect necrosis efficiency.

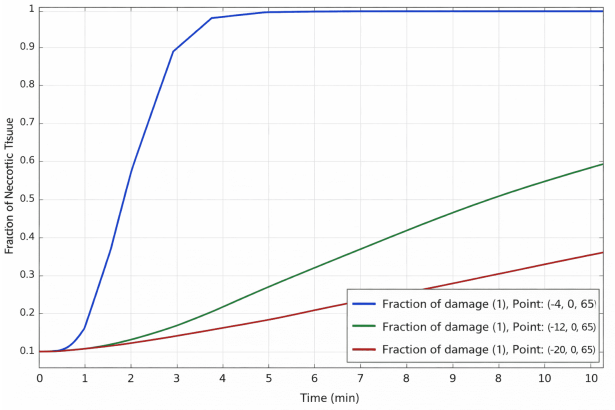

Figure 8. Fraction of necrotic tissue over time during microwave ablation

Figure 9 presents the same evaluation for radiofrequency application. Similarly, increasing the distance to the applicator reduces the rate of necrosis formation; this indicates that the spatial distribution of energy accumulation is determined by the heat conduction/convection balance. This comparison reveals that the two methods produce different necrosis geometries under the same boundary conditions, but the "distance-increase → damage-decrease" trend is maintained in both.

This validation step demonstrates that the necrosis output, sensitive to the presence of vessels, can be generated in accordance with the magnitudes reported in the literature. The agreement achieved at this stage provides a basis for confidently interpreting the differences arising from changes in vessel diameter and flow conditions in subsequent analyses.

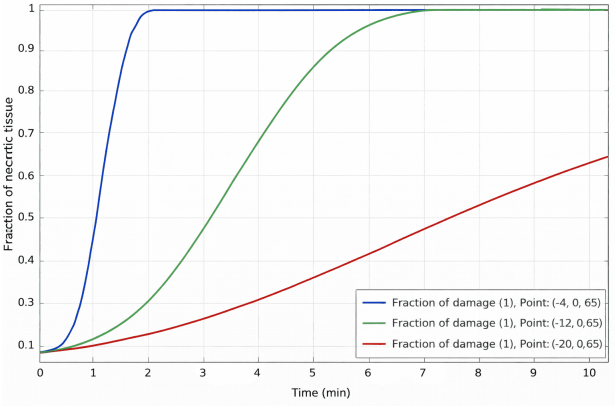

Figure 9. Faction of necrotic tissue over time during radiofrequency ablation

4 Conclusion

In this study, radiofrequency and microwave ablation methods were numerically investigated in the thermal treatment of liver tumors, considering the heat-sink effects originating from blood vessels. This trend is consistent with the ability of microwave energy to sustain volumetric heating and, when heating rates are sufficiently high, to mitigate heat-sink effects from nearby vessels. The heat-sink effects are larger for radiofrequency ablation than for microwave ablation; based on Table 2, the vessel-induced reduction in necrosis is 34.08% for radiofrequency ablation and 18.96% for microwave ablation, corresponding to an approximately 1.80-fold larger effect in radiofrequency. These findings support the view that convective heat removal by large vessels can affect radiofrequency and microwave ablation to different degrees, and that vascular geometry should be considered during treatment planning.

Geometric results indicate a tendency towards a more directional and focused heat/necrosis distribution in microwave ablation applications, and a more symmetrical distribution in radiofrequency applications. The fact that the necrosis area exhibits an elliptical character in microwave and a nearly spherical character in radiofrequency reflects the modality-dependent nature of energy accumulation and area distribution. This difference increases the value of numerical modeling, especially for evaluating which method works more safely with which placement and parameters in lesions near vessels. The results suggest that the cooling effect of the vessels may limit the adequacy of

necrosis, and the magnitude of this effect varies with the type of energy applied. In this context, expanding similar analyses under different vessel diameters, flow regimes, and tissue heterogeneity in future studies will contribute to defining thresholds and safety margins that can be transferred to clinical planning.

Author Contributions

Conceptualization, M.M.; methodology, M.M. and M.K.Y.; software, M.M.; validation, M.M.; formal analysis, M.M.; investigation, M.M. and M.K.Y.; data curation, M.M.; writing—original draft preparation, M.M. and M.K.Y.; writing—review and editing, M.K.Y..; visualization, M.M. and M.K.Y. All authors have read and agreed to the published version of the manuscript.

Data Availability

The data used to support the findings of this study are available from the corresponding author upon request.

Conflicts of Interest

The authors declare no conflict of interest.

References

[1] H. Qiao, A. Sohail, P. Kim, F. Hübner, and T. J. Vogl, "Intelligent ensemble learning-enhanced finite element modeling for precision thermal ablation in cancer therapy," *Comput. Methods Programs Biomed.*, vol. 274, p. 109157, 2026. https://doi.org/10.1016/j.cmpb.2025.109157

[2] M. De Melo Antunes, I. Burgers, V. Ozenne, L. Nardone, M. Seidensticker, O. Dietrich, M. Desclides, B. Quesson, A. Kusiak, S. M. M. de Lima e Silva *et al.*, "New analytical and hybrid heat transfer models for thermal ablation procedures validated by MRI thermometry," *Int. J. Hyperthermia*, vol. 42, no. 1, 2025. https://doi.org/10.1080/02656736.2025.2594943

[3] S. Tungjitkusolmun, S. T. Staelin, D. Haemmerich, J. Z. Tsai, H. Cao, J. G. Webster, F. T. Lee, D. M. Mahvi, and V. R. Vorperian, "Three-dimensional finite-element analyses for radio-frequency hepatic tumor ablation," *IEEE Trans. Biomed. Eng.*, vol. 49, no. 1, pp. 3–9, 2002. https://doi.org/10.1109/10.972834

[4] N. Vaidya, M. Baragona, V. Lavezzo, R. Maessen, and K. Veroy, "Simulation study of the cooling effect of blood vessels and blood coagulation in hepatic radio-frequency ablation," *Int. J. Hyperthermia*, vol. 38, no. 1, pp. 95–104, 2021. https://doi.org/10.1080/02656736.2020.1866217

[5] G. C. van Erp, P. Hendriks, A. Broersen, C. A. Verhagen, F. Gholamiankhah, J. Dijkstra, and M. C. Burgmans, "Computational modeling of thermal ablation zones in the liver: A systematic review," *Cancers*, vol. 15, no. 23, p. 5684, 2023. https://doi.org/10.3390/cancers15235684

[6] A. Alemaryeen and S. Noghanian, "A survey of the thermal analysis of implanted antennas for wireless biomedical devices," *Micromachines*, vol. 14, no. 10, p. 1894, 2023. https://doi.org/10.3390/mi14101894

[7] M. Bendahmane, Y. Ouakrim, Y. Ouzrour, and M. Zagour, "Mathematical study of a new coupled electro-thermo radiofrequency model of cardiac tissue," *Commun. Nonlinear Sci. Numer. Simul.*, vol. 139, p. 108281, 2024. https://doi.org/10.1016/j.cnsns.2024.108281

[8] Z. Fang, H. Wei, H. Zhang, M. A. J. Moser, W. Zhang, Z. Qian, and B. Zhang, "Radiofrequency ablation for liver tumors abutting complex blood vessel structures: Treatment protocol optimization using response surface method and computer modeling," *Int. J. Hyperthermia*, vol. 39, no. 1, pp. 733–742, 2022. https://doi.org/10.1080/02656736.2022.2075567

[9] D. Lim, B. Namgung, D. G. Woo, J. S. Choi, H. S. Kim, and G. R. Tack, "Effect of input waveform pattern and large blood vessel existence on destruction of liver tumor using radiofrequency ablation: Finite element analysis," *J. Biomech. Eng.*, vol. 132, no. 6, p. 061003, 2010. https://doi.org/10.1115/1.4001029

[10] E. De Vita, F. De Tommasi, C. Massaroni, A. Iadicicco, E. Faiella, M. Carassiti, R. F. Grasso, E. Schena, and S. Campopiano, "Investigation of the heat sink effect during microwave ablation in hepatic tissue: Experimental and numerical analysis," *IEEE Sens. J.*, vol. 21, no. 20, pp. 22 743–22 751, 2021. https://doi.org/10.1109/JSEN.2021.3107220

[11] B. Zhang, M. A. J. Moser, E. M. Zhang, Y. Luo, and W. Zhang, "Numerical analysis of the relationship between the area of target tissue necrosis and the size of target tissue in liver tumours with pulsed radiofrequency ablation," *Int. J. Hyperthermia*, vol. 31, no. 7, pp. 715–725, 2015. https://doi.org/10.3109/02656736.2015.1058429

[12] M. Mohammadpour and B. Firoozabadi, "High intensity focused ultrasound (HIFU) ablation of porous liver: Numerical analysis of heat transfer and hemodynamics," *Appl. Therm. Eng.*, vol. 170, p. 115014, 2020. https://doi.org/10.1016/j.applthermaleng.2020.115014

[13] S. Y. Choi, B. K. Kwak, and T. Seo, "Mathematical modeling of radiofrequency ablation for varicose veins," *Comput. Math. Methods Med.*, vol. 2014, p. 485353, 2014. https://doi.org/10.1155/2014/485353

[14] P. Rattanadecho and P. Keangin, "Numerical study of heat transfer and blood flow in two-layered porous liver tissue during microwave ablation process using single and double slot antenna," *Int. J. Heat Mass Transf.*, vol. 58, no. 1–2, pp. 457–470, 2013. https://doi.org/10.1016/j.ijheatmasstransfer.2012.10.043

[15] Y. L. Shao, B. Arjun, H. L. Leo, and K. J. Chua, "A computational theoretical model for radiofrequency ablation of tumor with complex vascularization," *Comput. Biol. Med.*, vol. 89, pp. 282–292, 2017. https://doi.org/10.1016/j.compbiomed.2017.08.025

[16] T. Kröger, I. Altrogge, T. Preusser, P. L. Pereira, D. Schmidt, A. Weihusen, and H. O. Peitgen, "Numerical simulation of radio frequency ablation with state dependent material parameters in three space dimensions," in *International Conference on Medical Image Computing and Computer-Assisted Intervention*, Copenhagen, Denmark, 2006, pp. 380–388. https://doi.org/10.1007/11866763_47

[17] S. Payne, R. Flanagan, M. Pollari, T. Alhonnoro, C. Bost, D. O'Neill, T. Peng, and P. Stiegler, "Image-based multi-scale modelling and validation of radio-frequency ablation in liver tumours," *Philos. Trans. R. Soc. A*, vol. 369, no. 1954, pp. 4233–4254, 2011. https://doi.org/10.1098/rsta.2011.0240

[18] C. Audigier, T. Mansi, H. Delingette, S. Rapaka, V. Mihalef, P. Sharma, D. Carnegie, E. Boctor, M. Choti, A. Kamen *et al.*, "Lattice boltzmann method for fast patient-specific simulation of liver tumor ablation from CT images," in *International Conference on Medical Image Computing and Computer-Assisted Intervention*, London, United Kingdom, 2013, pp. 323–330. https://doi.org/10.1007/978-3-642-40760-4_41

[19] J. Chiang, P. Wang, and C. L. Brace, "Computational modelling of microwave tumour ablations," *Int. J. Hyperthermia*, vol. 29, no. 4, pp. 308–317, 2013. https://doi.org/10.3109/02656736.2013.799295

[20] K. Pillai, J. Akhter, T. C. Chua, M. Shehata, N. Alzahrani, I. Al-Alem, and D. L. Morris, "Heat sink effect on tumor ablation characteristics as observed in monopolar radiofrequency, bipolar radiofrequency, and microwave, using ex vivo calf liver model," *Medicine*, vol. 94, no. 9, p. e580, 2015. https://doi.org/10.1097/MD.0000000000000580

[21] COMSOL AB, "Hepatic tumor ablation," Heat Transfer Module Application Library, COMSOL Multiphysics 6.0, 2022.

[22] H. H. Pennes, "Analysis of tissue and arterial blood temperatures in the resting human forearm," *J. Appl. Physiol.*, vol. 1, no. 2, pp. 93–122, 1948. https://doi.org/10.1152/jappl.1948.1.2.93

[23] X. Yuan, J. Fu, Y. Mao, J. Li, Y. Zhang, Y. Zhao, and H. Zhang, "Advances in bioheat transfer models for hyperthermia: A comprehensive review and future directions," *Results Eng.*, p. 107499, 2025. https://doi.org/10.1016/j.rineng.2025.107499

[24] M. H. Tehrani, M. Soltani, F. M. Kashkooli, and K. Raahemifar, "Use of microwave ablation for thermal treatment of solid tumors with different shapes and sizes—A computational approach," *PLoS One*, vol. 15, no. 6, p. e0233219, 2020. https://doi.org/10.1371/journal.pone.0233219

[25] C. C. R. Chen, M. I. Miga, and R. L. Galloway, "Optimizing electrode placement using finite-element models in radiofrequency ablation treatment planning," *IEEE Trans. Biomed. Eng.*, vol. 56, no. 2, pp. 237–245, 2009. https://doi.org/10.1109/TBME.2008.2010383

[26] B. Radjenović, M. Sabo, L. Šoltes, M. Prnova, P. Čičak, and M. Radmilović-Radjenović, "On efficacy of microwave ablation in the thermal treatment of an early-stage hepatocellular carcinoma," *Cancers*, vol. 13, no. 22, p. 5784, 2021. https://doi.org/10.3390/cancers13225784

[27] M. Radmilović-Radjenović, N. Bošković, and B. Radjenović, "Computational modeling of microwave tumor ablation," *Bioengineering*, vol. 9, no. 11, p. 656, 2022. https://doi.org/10.3390/bioengineering9110656

[28] IT'IS Foundation, "Tissue properties database v3.0," 2021. https://doi.org/10.13099/VIP21000-03-0

[29] J. W. Valvano, J. R. Cochran, and K. R. Diller, "Thermal conductivity and diffusivity of biomaterials measured with self-heated thermistors," *Int. J. Thermophys.*, vol. 6, pp. 301–311, 1985. https://doi.org/10.1007/BF00522151

[30] U. Zurbuchen, C. Holmer, K. S. Lehmann, T. Stein, A. Roggan, C. Seifarth, H. J. Buhr, and J. P. Ritz, "Determination of the temperature-dependent electric conductivity of liver tissue ex vivo and in vivo: Importance for therapy planning for the radiofrequency ablation of liver tumours," *Int. J. Hyperthermia*, vol. 26, no. 1, pp. 26–33, 2010. https://doi.org/10.3109/02656730903436442

[31] U. Zurbuchen, F. Poch, O. Gemeinhardt, M. E. Kreis, S. M. Niehues, J. L. Vahldieck, and K. S. Lehmann, "Determination of the electrical conductivity of human liver metastases: Impact on therapy planning in the radiofrequency ablation of liver tumors," *Acta Radiol.*, vol. 58, no. 2, pp. 164–169, 2017. https://doi.org/10.1177/0284185116639765

[32] F. Duck, *Physical Properties of Tissues: A Comprehensive Reference Book*. Academic Press, 2013.

[33] S. N. Mohapatra and D. W. Hill, "The changes in blood resistivity with haematocrit and temperature," *Eur. J. Intensive Care Med.*, vol. 1, pp. 153–162, 1975. https://doi.org/10.1007/BF00624433

[34] N. C. Hightower, "Resistivity and permittivity characteristics of human blood plasma during coagulation," Ph.D. dissertation, Georgia Institute of Technology, 1970.

[35] A. H. Negussie, A. Partanen, A. S. Mikhail, S. Xu, N. Abi-Jaoudeh, S. Maruvada, and B. J. Wood, "Thermochromic tissue-mimicking phantom for optimisation of thermal tumour ablation," *Int. J. Hyperthermia*, vol. 32, no. 3, pp. 239–243, 2016. https://doi.org/10.3109/02656736.2016.1145745